Available online at www.sciencedirect.com
ScienceDirect
International Journal of Heat and Mass Transfer 51 (2008) 539–552
International Journal of HEAT and MASS TRANSFER
www.elsevier.com/locate/ijhmt

Effective thermal conductivity of moistened insulation materials as a function of temperature

F. Ochs *, W. Heidemann, H. Müller-Steinhagen [1]

Institute of Thermodynamics and Thermal Engineering, University of Stuttgart, Pfaffenwaldring 6, 70569 Stuttgart, Germany

Received 16 November 2006; received in revised form 8 May 2007
Available online 16 July 2007

Abstract

Seasonal heat stores for waste heat applications or solar assisted district heating systems require thermal insulation in order to minimize heat losses. The insulation of these thermal energy stores is exposed to environmental influences. Especially the insulation of buried tank or pit heat stores may degrade due to increased moisture content caused by penetrating water (vapour). The effective thermal resistance of insulation materials decreases with increasing temperature and moisture content. Hence, thermal losses may become higher than the design values.

For the insulation of buried heat stores bulk materials are more suitable than sheets. However, the availability of measured data of the thermal conductivity of bulk insulation at higher temperatures and at elevated moisture contents is poor. Models for the thermal conductivity given in the VDI Heat Atlas and elsewhere have to be modified in order to obtain good agreement between calculated and measured data of the thermal conductivity of porous materials with partially closed and thus for water inaccessible pores.

This paper gives a detailed description of modelling and measurement of the effective thermal conductivity of porous bulk materials at temperatures up to 80 °C and moisture contents below free water saturation.

Keywords: Effective thermal conductivity; Insulation; Porous materials; Modelling and measurement; Hygrothermal modelling; Heat and moisture transfer

1. Introduction

Seasonal heat storage offers a great potential for substituting fossil fuels using waste heat from cogeneration heat and power plants (CHP) or solar energy for water preparation and space heating. Large-scale seasonal stores in (solar assisted) district heating systems have in comparison to decentralised heating systems lower specific investment costs and reduced relative thermal losses. Storage dimensions range from some 100 m^3 up to more than 10,000 m^3. In the majority of demonstration projects the heat stores are buried or partially buried for space and optical reasons. A detailed description of German projects with seasonal store from the years 1994 to 2006 is given in [1–4]. An overview about international projects with seasonal heat store can be found in [5,6]. Besides Germany, Switzerland [7], Denmark [8,9] and Sweden [10] did extensive research on seasonal heat stores.

Whereas, in earlier projects, sheets of rock wool, mineral wool or polystyrene (EPS or XPS) have been installed at the walls and on the cover, the more recent stores are insulated with bulk insulation like expanded glass granules (EGG) or foam glass gravel (FGG). The investigated insulation materials are shown in Fig. 1. Particularly for large stores installation of bulk material by pouring or by air injecting is much more cost- and time-effective than mounting insulation sheets or plates. Recent projects like the hot water tank store in Munich (Germany) will be insulated

* Corresponding author. Tel./fax: +49 711 685 6 3278.
E-mail address: ochs@itw.uni-stuttgart.de (F. Ochs).
[1] Also at Institute of Technical Thermodynamics, DLR Stuttgart, Pfaffenwaldring 38-40, 70569 Stuttgart, Germany.

0017-9310/$ - see front matter © 2007 Elsevier Ltd. All rights reserved.
doi:10.1016/j.ijheatmasstransfer.2007.05.005

Nomenclature

Latin symbols

a	fraction of poorly conductive layers (–)
A	area (m^2)
b	fraction of moistened pores (–)
c_p	specific heat capacity ($J\,(kg\,K)^{-1}$)
c	approximation factor for $b(u)$, model II (–)
c_{rad}	radiation constant ($W\,m^{-1}\,K^{-4}$)
d	diameter (m)
D	diffusion coefficient ($m^2\,s^{-1}$)
g	acceleration due to gravity ($m\,s^{-2}$)
h_v	latent heat of evaporation ($kJ\,kg^{-1}$)
l	length (m)
m_1, m_2	parameter for $b(u)$, model III (–)
p	pressure (Pa)
$\dot{Q}$	heat flow rate
R	gas constant ($J\,(kg\,K)^{-1}$)
T	absolute temperature (K)
u	(absolute) moisture content ($kg\,m^{-3}$)
V	volume (m^3)
X	relative moisture content (–)

Greek symbols

β	coefficient of expansion (K^{-1})
Δ	difference (–)
ε	emissivity coefficient (–)
η	dynamic viscosity ($kg\,(m\,s)^{-1}$)
ϑ	Celsius temperature (°C)
λ	thermal conductivity ($W\,(m\,K)^{-1}$)
μ	water vapour diffusion resistance factor (–)
ν	kinematic viscosity ($m^2\,s^{-1}$)
ρ	(bulk) density ($kg\,m^{-3}$)
σ	surface tension ($N\,m^{-1}$)
σ_S	Boltzmann constant ($W\,m^{-2}\,K^{-4}$)
ϕ	relative humidity (–)
χ	empirical factor (–)
Ψ	porosity (void fraction) (–)
Ψ_w	volume related liquid water content (–)

Subscripts

I, II	parallel, serial layer
a	air
amb	ambient
av	average
b	bulk
cl	closed
diff	diffusion
eff	effective
exp	experimental
fs	free saturation
g	grain (particle)
max	maximum
m	mean
meas	measured
op	open
p	pore
pg	pore gas
R	rated
rad	radiation
ref	reference
s	solid
sat	saturation
SP	set point
v	vapour
w	water

Dimensionless numbers

$Ra = Gr \cdot Pr$ Rayleigh number (–)

$Gr = \frac{g \cdot \beta \cdot \Delta\vartheta \cdot l^3}{\nu^2}$ Grashof number (–)

$Pr = \frac{\nu \cdot \rho \cdot c}{\lambda}$ Prandtl number (–)

using expanded glass granules and foam glass gravel (see [11]). Only the most recent projects have bottom insulation, which is either made of sheets of foam glass or of compacted foam glass gravel due to the requirements concerning pressure resistance.

Protection from rain and surface water is of importance when choosing a construction or installation procedure, as for large stores mounting the installation can take several days and even weeks. However, moisture penetration from the inside of the store by diffusion and from the surrounding soil by diffusion and convection into the thermal insulation cannot be completely prevented.

Increased moisture content, in particular at the high operating temperatures of up to 100 °C, results in a decreased thermal resistance of the insulation and, consequently, in increased thermal losses of the heat store. The thermal losses measured during operation of the pilot and research (seasonal) heat stores are in most cases higher than the simulated values. For these transient simulations constant values for thermal conductivity according to DIN 4108 [12] have been used. The assumption of constant material properties (thermal conductivity of insulation and of surrounding ground, water vapour resistance index of liner) leads to wrong results as will be demonstrated in this paper. Table 1 shows calculated and measured values of thermal losses of some research and demonstration projects of solar assisted district heating systems with buried seasonal heat store. Actual thermal losses are 30–50% higher than the design values. In one case the thermal losses are even three times higher (see [24]).

There are several reasons that cause the high thermal losses. Poor stratification causes higher internal losses.

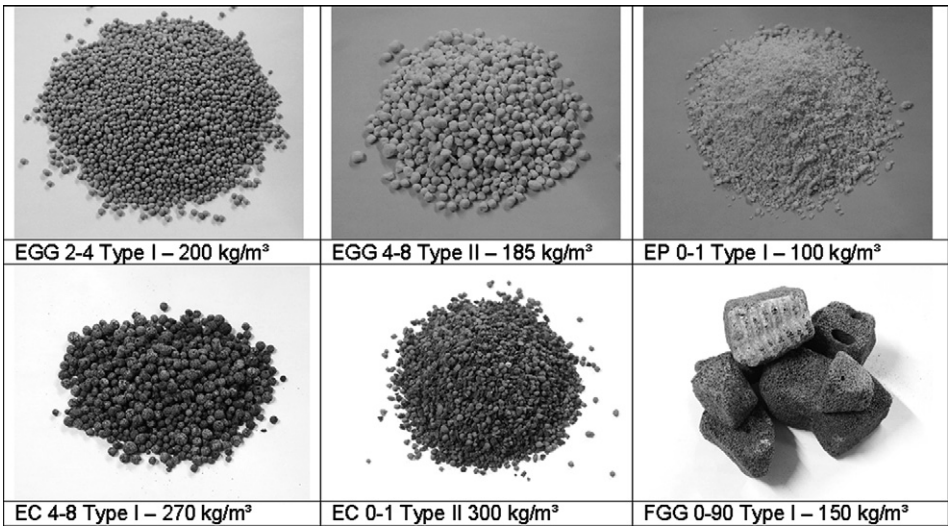

Fig. 1. Bulk insulation materials, expanded glass granules (EGG), expanded perlite (EP), expanded clay (EC) and foam glass gravel (FGG).

Table 1
Comparison of design data and measured values of selected research and demonstration tank stores and pit heat stores

Location/name	Country	References	Date	V (m^3)	A (m^2)	$\dot{Q}_{meas}$ (MWh/a)	$\dot{Q}_{meas}/\dot{Q}_{design}$ (–)	A/V (1/m)	ΔT^h (K)	$\dot{Q}/(\Delta T \cdot A)$ (kWh/(K m^2 a))
Tank heat stores										
Studsvik	S	[13]	1978	1200	450	n/a.	1.07–1.3	0.38	n/a.	n/a.
Lombohov	S	[13]	1980	10 000	1750	250	3	0.18	n/a.	n/a.
Hamburg	D	[2]	1996	4500	1650	360–430	3.8–4.5	0.37	42	5.7
Friedrichshafen	D	[2,14]	1996	12 000	2796	320–360	1.5–1.6	0.23	49	2.5
Ilmenau [a]	D	[15]	1998	300	262	n/a.	1.2	1.14	n/a.	n/a.
Hannover	D	[2,16]	2000	2750	1135	90–100	1.3–1.4	0.41	33	2.5
Crailsheim	D	[17]	2005	100	141	n/a.	n/a.	1.41	n/a.	n/a.
Crailsheim [b]	D	[11,18]	2007	480	362	–	–	0.75	–	–
Munich [b]	D	[11,18]	2007	6000	1800	–	–	0.30	–	–
Pit heat stores										
Stuttgart (GW)[c]	D	[19]	1985	1050	835	27	<1	0.84	8	0.4
Chemnitz (GW)[d]	D	[20]	1997	8000	3375	n/a.	1.4	0.42	n/a.	n/a.
Steinfurt (GW)[e]	D	[2,21,22]	1999	1500	1147	70–90	n/a.	0.77	26	2.7
Marstal (HW)[f]	DK	[23]	2003	10 000	5600	338	n/a.	0.56	22	0.6

n/a, not available.
[a] Extrapolation of a five month period.
[b] Construction in 2006/2007.
[c] 462 h simulation, operation with heat pump, $T_{av,storage} = 16.5$ °C.
[d] Construction in 1996, extrapolation of 8 week data.
[e] Thermal losses of store including connecting pipes.
[f] A period of 6 month according to [9].
[h] Average storage temperature minus average ambient/ground temperature $\Delta T = T_{m,s} - T_{m,a}$.

Higher thermal losses to the ground resulting from increased temperature at the bottom region of the store as a consequence of high return temperatures contribute furthermore to higher thermal losses. Insufficient knowledge about the boundary conditions (ground water level and flow) also may contribute to an underestimation of the thermal losses. However, the main reason may be moistened insulation. The quality of the envelope with respect to protection against moisture penetration is often deficient.

The availability of measured thermal conductivity data of (bulk) insulation at higher temperatures and at elevated moisture contents is poor. The objective of this work is to fill this gap.

2. Material characterisation

Available insulation materials can be divided into inorganic artificial products like expanded glass and foam glass, which are made of recycled glass (~98%, [25]) and

inorganic natural products like expanded clay and expanded perlite. Bims, vermiculite and lava stones also belong in this group, but are not considered in this work. Organic materials (natural and artificial) are not considered, as pressure resistance is not given in the required temperature range. Bulk densities range (ρ) from 100 kg/m^3 to almost 400 kg/m^3, with rated thermal conductivities (λ_R) in the range from 0.05 W/(m K) to 0.12 W/(m K) according to DIN 4108 [12] The grain (particle) size (d) of the investigated bulk materials is 0–1 mm, 2–4 mm, 4–8 mm or 8–16 mm for expanded glass, expanded clay and expanded perlite and 0/20 mm, 0/90 or 10/50 mm for foam glass gravel (see Table 2).

For a model of the thermal conductivity, knowledge about the pore fraction and the properties of the solid particles is required. In the presence of moisture further material characteristics like pore structure or hygric properties have to be considered. The free water saturation content (u_{fs}) and the moisture storage function ($u(\phi)$) are the most important characteristics. For the above mentioned materials only few publications may be found in the literature [26,27]. The pore fraction and pore size distribution and the density of the solid are measured according to the standards using mercury porosimetry (DIN 66133, [28]) or helium pycnometry (DIN 66135, [29]), respectively. Both methods require major effort and expenses. As has been demonstrated by Faust (see [26]), the results obtained by simplified experiments show good agreement with measured results obtained with experimental set-ups according to DIN specifications. The density and the thermal conductivity of the solid materials, listed in Table 3, are available in the literature (see [12,26,27,30,31] or [32]).

Table 2
Bulk insulation material, grain size (d) and manufacturer information on density (ρ) and rated thermal conductivity (λ_R)

Nr.	Material	Grain size d (mm)	Density ρ (kg/m^3)	Rated thermal conductivity λ_R (W/(m K))
Expanded glass				
1	EGG type I	2–4	190	0.07
2	EGG type II	2–4	190	0.08
3	EGG type II	4–8	180	0.08
4	EGG type II	8–16	140	0.08
Expanded clay				
5	EC type I	4–8	300	0.10
6	EC type I	4–8	325	0.10
7	EC type I	1–4	300	0.08
8	EC type II	0–1	330	n/a.
Expanded perlite				
9	EP type I	0–1	90	0.05
Foam glass				
10	FGG type I	0–20	150	0.06
10a	FGG type I	0–90	150	0.08/0.14
11	GFG type II	10–50	195	0.09
12	GFG type III	10–50	170	0.08

λ_R: thermal conductivity, dry at 10 °C according to DIN 4108 [12] or manufacturer data. EGG: expanded glass granules. EC: expanded clay. EP: expanded perlite. FGG: foam glass gravel. GFG: glass foam gravel. ρ_{grain}(FGG type I) = 200 kg/m^3. ρ_{grain}(GFG type II) = 225 kg/m^3.

Table 3
Thermo-physical properties of solid particles

Material	Density ρ_s (kg/m^3)	Thermal conductivity λ_s (W/(m K))	Specific heat capacity c_p (kJ/(kg K))	Insulation	References
Glass	2480	1.16	0.8	EGG, FGG	[12,26,32][a]
Clay	2650	3.44	0.6	EC	[27]
Perlite	2000	1.30	0.8	EP	[12][b]
Stone/sand/chalk	2700	2.70	0.8	Rock wool	[12]
PUR/PIR	1050	0.58	1.3	PUR	[31]
Styrol	1050	0.18	1.8	XPS, EPS	[31]

[a] About 98% recycled glass, average value for glass is taken.
[b] No reliable literature data available.

When modelling the effective thermal conductivity as a function of the moisture content the fraction of open pores (accessible for water) and closed pores (non-accessible for water) is required. The total (or bulk) pore fraction (Ψ) can be determined using the total (bulk) density (ρ) and the density of the solid (ρ_s) according to the following equation.

$$\Psi = 1 - \frac{\rho}{\rho_s} \tag{1}$$

The macro porosity, which corresponds to the fraction of the voids between the grains (Ψ_{macro}) and the fraction of closed pores (Ψ_{cl}) can be measured according to the method described in [33]:

$$\Psi_{op} = \Psi - \Psi_{cl} = \Psi_{macro} + \Psi_{micro} \tag{2}$$

The open porosity (Ψ_{op}) consists of the macro porosity (Ψ_{macro}) and the micro porosity (Ψ_{micro}). The micro porosity is the fraction of open and thus for water accessible pores of the grain.

$$\Psi_{macro} = 1 - \frac{\rho_{macro}}{\rho_s} \tag{3}$$

For a single grain, the porosity can be calculated using the total porosity (Ψ) and the macro porosity (Ψ_{macro}).

$$\Psi_g = \frac{\Psi - \Psi_{macro}}{1 - \Psi_{macro}} \tag{4}$$

SEM photographs of a grain of expanded glass granules (2–4 mm, type I and 2–4 mm type II) are shown in Fig. 2. The different pore structure and pore distribution of the grain is obvious. Graphical analysis of the SEM pictures yield a grain porosity, which is about 2% points lower than the value obtained by measurements according to [33] as can be seen in Table 4. By means of mercury porosimetry (see [26]) yet a slightly higher value was measured.

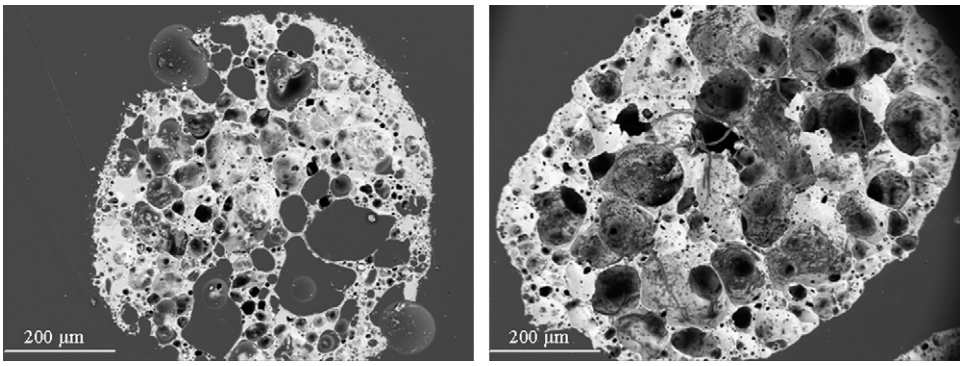

Fig. 2. Pore structure of porous bulk materials: SEM picture of EGG 2.4 mm type I and EGG 2–4 mm type II embedded in epoxy resin.

Table 4
Total porosity of the grain (Ψ_g) of expanded glass granules (EGG) with different grain diameters, of foam glass gravel (FGG) 0–90 mm and of expanded clay (EC) 4–8 mm

	EGG 2–4 type I	EGG 2–4 type II	EGG 4–8 type II	EGG 8–16 type II	FGG 0–90 type I	EC 4–8 type I
SEM, see Fig. 2	0.86	0.86	0.86	0.87	0.87	n/a.
Walz [33]	0.88	0.88	0.88	0.89	0.91	0.76
Faust [26]	0.89	n/a.	n/a.	n/a.	n/a.	0.58

Comparison of different sources: SEM picture analysis, mercury porosimetry from Faust [26] and own measurement according to the method suggested by Walz, see Ref. [33]. n/a.: not available.

Table 5 lists the mechanical and hygric material properties, determined as described above in Eqs. (1)–(4).

The free saturation has been determined as the drain weight according to DIN EN 13755 [34]. In Table 5 the free saturation water content (u_{fs}) is compared with the maximum water content (u_{max}) which is defined by Eq. (5):

$$u_{max} = \Psi_{op} \cdot \rho_w \quad (5)$$

In Table 5 also the pore structure and pore distribution of the bulk insulation are compared. Although values of the total or bulk porosity of the porous materials are similar, (in the range from 0.87 to 0.95) the fraction of closed pores differs from 0.25 to 0.44. The maximum water content varies between 500 and 700 kg/m^3 and the free saturation water content is in a range between 300 and 550 kg/m^3.

Table 5
Grain size (d), measured bulk density (ρ), bulk or total (Ψ) porosity, open (Ψ_{op}) and macro porosity (Ψ_{macro}) and porosity of the grain consisting of micro porosity (Ψ_{micro}) and closed pore porosity ($\Psi_{g,cl}$) measured according to Refs. [33] or [34] as well as free saturation (u_{fs}), and maximum water content (u_{max})

Material	Grain size d (mm)	Density (ρ) (kg/m^3)	Total porosity Ψ (–)	Open porosity Ψ_{op} (–)	Macro porosity Ψ_{macro} (–)	Grain porosity Ψ_{grain} (–)	Free saturation water content u_{fs} (kg/m^3)	Maximum water content u_{max} (kg/m^3)
			Eq. (1)	Eq. (2)	Eq. (3)	Eq. (4)	Ref. [34]	Eq. (5)
Expanded glass								
EGG type I	2–4	200	0.92	0.61	0.38	0.88	550	610
EGG type II	2–4	190	0.93	0.57	0.38	0.88	515	570
EGG type II	4–8	185	0.93	0.61	0.42	0.88	500	610
EGG type II	8–16	150	0.94	0.65	0.46	0.89	400	650
Expanded clay								
EC type I	4–8	270	0.90	0.51	0.45	0.81	300	510
EC type I	4–8	380	0.87	0.54	0.47	0.76	345	540
EC type I	1–4	340	0.88	0.65	0.61	0.69	360	650
EC type II	0–1	300	0.89	0.57	0.54	0.77	360	570
Expanded perlite								
EP type I	0–1	100	0.95	0.51	0.48	0.90	370	510
Foam glass								
FGG type I	10–20	155	0.94	0.69	0.66	0.83	460	690
GFG type II	10–50	195	0.92	0.48	0.46	0.86	150	480

3. Modelling of the effective thermal conductivity

3.1. Modelling concepts

The VDI Heat Atlas [30] distinguishes between three types of models for the calculation of the thermal conductivity of porous materials. Type I regards the temperature and heat flux profile of two particles which are in contact (unity cell). It is the most complex model in terms of calculation effort. It has to be solved numerically and is hence seldom used. A simplification is represented by type III. Analogue to type I the unity cell is regarded, but instead of a grid of isotherms and heat flux lines either parallel isotherms or heat flux lines are considered. A frequently used representative is the model developed by Zehner, Bauer and Schlünder (see [35] for details). It describes the thermal conductivity very well, if secondary parameters like the thermal contact resistance or flattening effects are considered with priority.

However, when calculating the thermal conductivity of bulk material with porous grains with partially closed pores as a function of temperature and moisture content, the best results are achieved using a model based on type II. The porous material is mapped onto a combination of serial and parallel layers representing thermal resistances of the components as proposed by Krischer and Kast [36]. All primary parameters such as porosity, thermal conductivity of the fluid(s) and of the solid as well as the influence of radiation, which is a secondary parameter, are considered.

Convection can be neglected in the present investigation as, according to Zeitler [37], it only takes place when the Rayleigh number, defined in Eq. (6), exceeds the critical number $Ra_{crit} > 1708$:

$$Ra = Gr \cdot Pr = \frac{g \cdot \beta_{pg} \cdot \Delta T_p \cdot d_{p,m}^3}{\nu_{pg} \cdot a_{pg}} \tag{6}$$

Even for coarse-grained materials with mean grain diameters of 12 mm the Rayleigh number remains smaller than the critical value under the given boundary conditions.

3.2. Modelling of the thermal conductivity of moistened porous materials

The thermal conductivity of moistened porous materials can be expressed in terms of an aggregation of serial and parallel layers consisting of solid (s), liquid water (w), humid air and dry air (a) see Fig. 3. Other pore gases such as CO_2 may be considered, too. The materials that have been investigated in the frame of this work have a fraction of 23–44% of closed pores (see Table 5). It is advantageous to consider the closed pores as an additional layer as will be shown later. This leads to a five layer model according to Fig. 4.

The summation of the serial layers yields the maximum thermal conductivity.

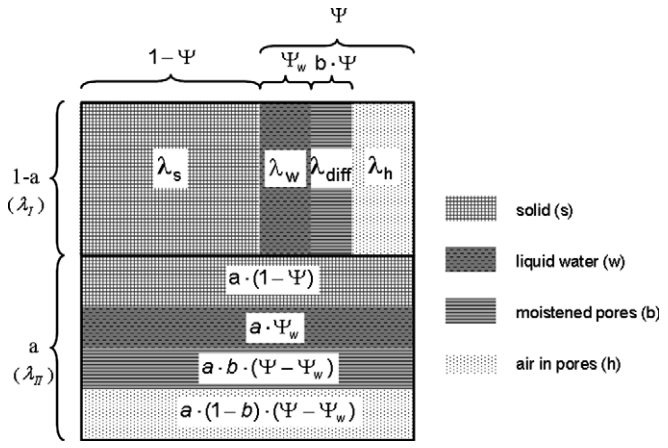

Fig. 3. Model for the calculation of the thermal conductivity of moistened materials according to Krischer and Kast [36].

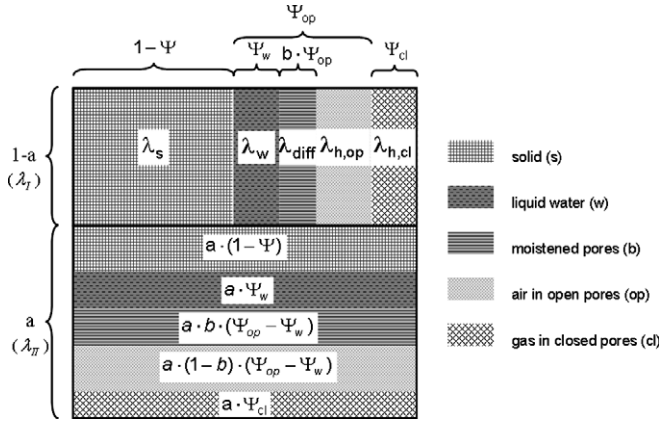

Fig. 4. Extended layer model, which takes into account the fraction of closed and thus by moisture unaffected pores.

$$\lambda_I = (1-\Psi)\cdot\lambda_s + \Psi_w\cdot\lambda_w + b\cdot(\Psi_{op}-\Psi_w)\cdot(\lambda_p+\lambda_{diff}) + (1-b)\cdot(\Psi_{op}-\Psi_w)\cdot\lambda_p + \Psi_{cl}\cdot\lambda_{p,cl} \tag{7}$$

The minimum thermal conductivity is obtained by adding the parallel layers, which are weighted with a. The maximum thermal conductivity in Eq. (8) is weighted accordingly with $(1-a)$.

$$\lambda_{II} = \left(\frac{1-\Psi}{\lambda_s} + \frac{\Psi_w}{\lambda_w} + \frac{b\cdot(\Psi_{op}-\Psi_w)}{\lambda_p+\lambda_{diff}} + \frac{(1-b)\cdot(\Psi_{op}-\Psi_w)}{\lambda_p} + \frac{\Psi_{cl}}{\lambda_{p,cl}}\right)^{-1} \tag{8}$$

The addition of the weighted maximum (λ_I) and minimum (λ_{II}) thermal conductivity results in the effective thermal conductivity (λ_{eff}) of the porous medium.

$$\lambda_{eff} = \frac{1}{\frac{1-a}{\lambda_I} + \frac{a}{\lambda_{II}}} \tag{9}$$

3.3. Modelling the thermal conductivity of dry materials

For dry materials with air as pore gas, the number of layers in the model is reduced to two: solid with the fraction $(1-\Psi)$ and air with the fraction (Ψ).

$$\lambda_{\mathrm{I}} = (1-\Psi)\cdot\lambda_{\mathrm{s}} + \Psi\cdot\lambda_{\mathrm{p}} \tag{10}$$

and correspondingly

$$\lambda_{\mathrm{II}} = \frac{1}{\frac{1-\Psi}{\lambda_{\mathrm{s}}} + \frac{\Psi}{\lambda_{\mathrm{p}}}} \tag{11}$$

The thermal conductivity of the solid can be measured according to a method proposed in [27] if literature data are not available. The solid phase of the investigated bulk materials is, with the exception of perlite, either glass or clay.

The effective thermal conductivity of the pore (p) consists of a contribution of molecular conduction of the pore gas (pg) and a contribution due to radiation (rad).

$$\lambda_{\mathrm{p}} = \lambda_{\mathrm{pg}} + \lambda_{\mathrm{rad}} \tag{12}$$

In the present materials the pore gas is air. The thermal conductivity of air can be approximated using a second-order polynomial [36].

$$\lambda_{\mathrm{a}} = 0.0243 + 7.8421\cdot10^{-5}\vartheta - 2.0755\cdot10^{-8}\vartheta^2 \tag{13}$$

The effect of the radiation can be considered using Eq. (14).

$$\lambda_{\mathrm{rad}} = \frac{4\cdot\sigma_{\mathrm{s}}\cdot d_{\mathrm{m}}}{(2/\varepsilon)-1}T^3 \tag{14}$$

where σ_{s} is the blackbody radiation constant, ε the coefficient of emission of the particle surface, T the absolute temperature in K and d_{m} the pore diameter. As the coefficient of emission is not available in most of the cases, the parameters in Eq. (14) are lumped to the radiation constant (c_{rad}), which can be determined from the experiments.

$$\lambda_{\mathrm{rad}} = c_{\mathrm{rad}}\cdot T^3 \tag{15}$$

Using the Nelder–Mead method [38] the unknown parameters a and c_{rad} may be identified. The measured thermal conductivity of the (oven-) dry materials and the corresponding model predictions are plotted in Fig. 5. More details about the measurement method are given in Section 3.8.

The lowest thermal conductivity could be measured for expanded perlite with about 0.05 W/(m K) at 20 °C. The highest value is 0.10 W/(m K) for expanded clay. All investigated porous bulk materials show a (nearly) linear increase of the effective thermal conductivity with temperature.

The resulting fraction of serial layers (a) and the corresponding radiation constant (c_{rad}) of the examined insulation materials are compared in Table 6. The higher the radiation constant, the higher is the slope of thermal conductivity with respect to temperature. However, no direct agreement occurs between the slope of the best linear fit and the values of the radiation constant, as is shown in Table 6.

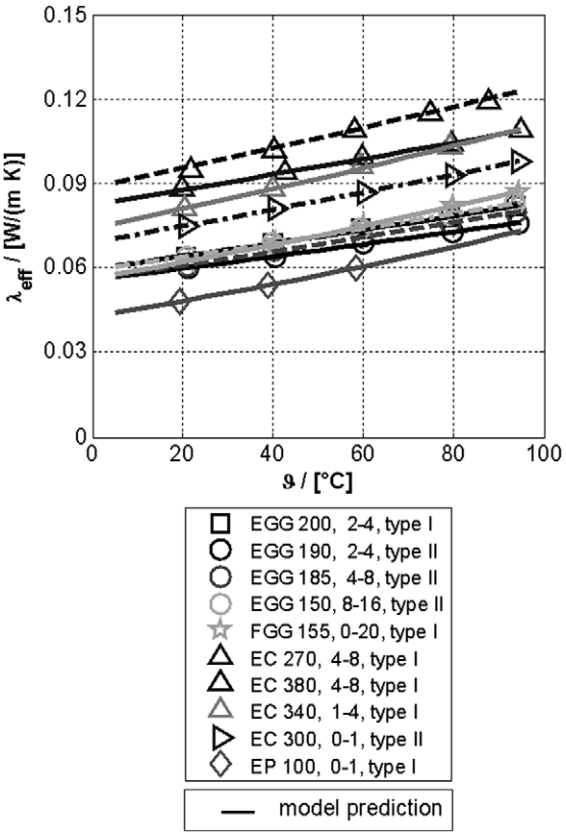

Fig. 5. Measured thermal conductivity (λ_{eff}) of bulk insulation material (marker) as a function of temperature (ϑ), and model predictions (lines).

3.4. Modelling of the influence of moisture as a function of temperature

In order to model the presence of moisture, the thermal conductivity of liquid water (λ_{w}) and of water saturated air ($\lambda_{\mathrm{a,sat}}$) in Eqs. (7) and (8) have to be calculated. The thermal conductivity of water can be represented by a third-order polynomial approach according to [36].

$$\lambda_{\mathrm{w}} = 0.557 + 0.0022\vartheta - 1.051\cdot10^{-5}\vartheta^2 + 1.081\cdot10^{-8}\vartheta^3 \tag{16}$$

The thermal conductivity of water vapour (v) as a function of temperature is given by Quast [39]:

$$\lambda_{\mathrm{v}} = \frac{1.713\cdot10^{-4}\cdot(1+0.0129\cdot T)\cdot\sqrt{T}}{1-\frac{80.95}{T}} \tag{17}$$

Ackermann [40] provides an equation for the thermal conductivity of water saturated air with the saturation pressure p_{sat} according to Eq. (33) at an absolute pressure of $p_{\mathrm{amb}} = 1$ bar.

$$\lambda_{\mathrm{a,sat}} = 0.5\cdot\left[p_{\mathrm{sat}}\cdot\lambda_{\mathrm{v}} + (1-p_{\mathrm{sat}})\cdot\lambda_{\mathrm{a}} + \frac{1}{\frac{p_{\mathrm{sat}}}{\lambda_{\mathrm{v}}} + \frac{1-p_{\mathrm{sat}}}{\lambda_{\mathrm{a}}}}\right] \tag{18}$$

Table 6
Fraction of serial and thus poor conductive layers (a) and corresponding values of the radiation constant (c_{rad}), determined using the Nelder–Mead iteration method, slope of the linear best fit ($d\lambda/d\vartheta$)

Material	Grain size d (mm)	Density ρ (kg/m^3)	Fraction of poor conductive layers a (–)	Radiation constant c_{rad} (10^{-10} W/(m K^4))	Slope $d\lambda/d\vartheta$ (10^{-3} W/(m K °C))
Expanded glass					
EGG type I	2–4	200	0.387	3.1	0.243
EGG type II	2–4	190	0.410	3.0	0.221
EGG type II	4–8	185	0.441	3.9	0.260
EGG type II	8–16	150	0.369	4.2	0.260
Expanded clay					
EC type I	4–8	270	0.297	1.0	0.278
EC type I	4–8	380	0.335	2.4	0.367
EC type I	1–4	340	0.431	3.4	0.284
EC type II	0–1	300	0.420	2.2	0.311
Expanded perlite					
EP type I	0–1	100	0.925	7.2	0.308
Foam glass					
FGG type I	10–20	155	0.424	5.6	0.340
GFG type II	10–50	195	0.152	11.1	0.492

The fraction of pores filled with liquid water can be estimated using the absolute moisture content (u).

$$\Psi_w = u/\rho_w \tag{19}$$

Depending on the temperature, a certain part of the total amount of water per volume (u) evaporates. Thus, the actual volume that is occupied by liquid water is reduced. In the maximum case this can be estimated by

$$u_{v,sat} = X_{sat} \cdot \rho_a \cdot \Psi_{op} \tag{20}$$

with the saturation vapour content (X_{sat})

$$X_{sat} = \frac{R_a}{R_v} \cdot \frac{p_{sat}}{p - p_{sat}} \tag{21}$$

3.5. Thermal conductivity due to pore diffusion

For the moistened pores, the conductive terms of the solid λ_s, of the water λ_w and of the dry air λ_a or saturated air $\lambda_{a,sat}$ are taken into account according to Eqs. (7) and (8). Additionally, heat transfer due to evaporation at the warm side of a pore and condensation at the opposite cold side of the pore occurs. The effective thermal conductivity due to pore diffusion (λ_{diff}) is modelled introducing an additional term, which is added to the thermal conductivity of the pore λ_p.

$$\lambda_{p,op} = \lambda_p + \lambda_{diff} \tag{22}$$

The term (λ_{diff}) describing the heat transport due to pore diffusion is expressed in different ways in the literature. Krischer [36] who developed the original model proposed:

$$\lambda_{diff} = \frac{D_v}{R_v \cdot T} \cdot \frac{p_{amb}}{p_{amb} - p_{sat}} \cdot \frac{dp_{sat}}{d\vartheta} \Delta h_v \tag{23}$$

In the VDI Heat Atlas ([41], chapter Mg 11) a similar correlation can be found.

$$\lambda_{diff} = \frac{D_v}{R_v^2 T^2} \frac{p_{amb}}{p_{amb} - p_{sat}} \Delta h_v^2 \tag{24}$$

De Vries [42] suggests the following correlation for the thermal conductivity due to pore diffusion.

$$\lambda_{diff} = D_v \cdot \frac{\partial \rho_{sat}}{\partial \vartheta} \cdot \Delta h_v \tag{25}$$

For the temperature dependent parameters, the vapour diffusion coefficient D_v and the saturation vapour pressure p_{sat}, different empirical correlations are suggested in the literature. While Krischer [36] applied the following empirical function

$$D_v = 23.4 \cdot 10^{-6} \left(\frac{T}{273}\right)^{2.3} \tag{26}$$

the VDI Heat Atlas [41] gives

$$D_v = \frac{2.252}{p_{amb}} \cdot \left(\frac{T}{273}\right)^{1.81} \tag{27}$$

The correlation widely used in soil physics is given in [43] according to measurements from Schirmer [44].

$$D_v = 2.31 \cdot 10^{-5} \frac{p_{amb}}{p_{amb} + p_v} \cdot \left(\frac{T}{273}\right)^{1.81} \tag{28}$$

Schirmer is cited by other authors with different correlations i.e., according to [45] with

$$D_v = 2.33 \cdot 10^{-5} \frac{p}{p_{amb}} \cdot \left(\frac{T}{273}\right)^{1.81} \tag{29}$$

or by Krischer [36] with

$$D_v = \frac{22.6 \cdot 10^{-6}}{p_{amb}\,[\text{bar}]} \cdot \left(\frac{T}{273}\right)^{1.81} \tag{30}$$

According to Vos (from [46]) the temperature dependence of D_v can be expressed as

$$D_v = (22.2 + 0.14 \cdot (T - 273.15)) \cdot 10^{-6} \quad (31)$$

And finally, according to the De Vries [42] approach, Eq. (25), the vapour diffusion coefficient is

$$D_v = 2.17 \cdot 10^{-5} \frac{p}{p_{amb}} \cdot \left(\frac{T}{T_0}\right)^{1.81} \quad (32)$$

The different approaches of the vapour diffusion coefficient (D_v) are plotted and compared in Fig. 6. Particularly, the correlation originally suggested by Schirmer (in [43]) deviates at temperatures above 50 °C if p_v is equal p_{sat}. In Fig. 7 thermal conductivities obtained by the Eqs. (23)–(25) are plotted as a function of the temperature using the appropriate vapour diffusion coefficients (Eqs. (25), (26) and (32)). Whereas, the equations according to Krischer and VDI Heat Altas provide similar results, the De Vries approach yields significant deviations above 70 °C.

Furthermore, different correlations for the vapour saturation pressure can be found in the literature. According to

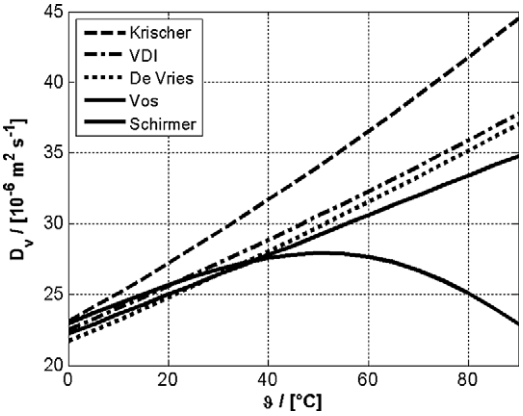

Fig. 6. Diffusion coefficient (D_v) of vapour in air as a function of the temperature (ϑ) according to various authors.

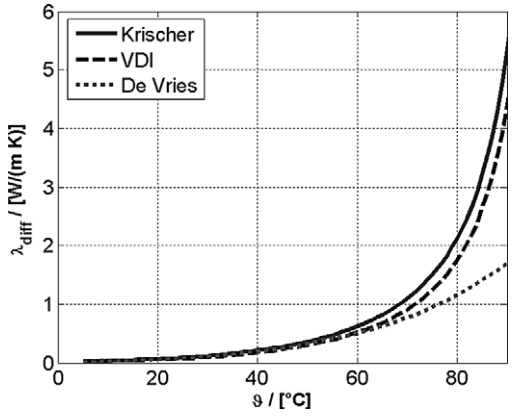

Fig. 7. Effective thermal conductivity (λ_{diff}) due to pore diffusion as a function of temperature (ϑ), according to Krischer and Kast [36], VDI Heat Atlas [41] and de Vries [42].

Magnus [47] the saturation pressure can be calculated in a temperature range from 0 °C to 109.9 °C using

$$p_{sat} = 610.8 \cdot \exp\left(\frac{17.08085 \cdot \vartheta}{234.175 + \vartheta}\right) \quad (33)$$

Using the Antoine correlation (in [48]) results in

$$p_s = 10^5 \cdot \exp\left(11.6834 - \frac{3816.44}{319.61 + \vartheta}\right) \quad (34)$$

The VDI Heat Atlas [41] gives the correlation

$$p_{sat} = \exp\left(23.462 - \frac{3978.205}{233.349 + \vartheta}\right) \quad (35)$$

The results obtained by Eqs. (33)–(35) do not deviate significantly. With the correlation originally used by Krischer (cf. Eq. (33) from [36]) the derivation of the saturation pressure in Eq. (23) yields

$$\frac{dp_{sat}}{d\vartheta} = \frac{2.44314 \cdot 10^6}{(234.175 + \vartheta)^2} \cdot \exp\left(\frac{17.08085 \cdot \vartheta}{234.175 + \vartheta}\right) \quad (36)$$

The gas constant of water vapour is $R_v = 461.5$ J/(kg K) and the specific heat of evaporation is $\Delta h_v = 2260$ kJ/kg.

In the following calculations, for the saturation pressure the correlation according to Magnus, Eq. (33), and for the diffusion coefficient the correlation from Krischer, Eq. (26), have been applied.

3.6. Approximation of the fraction of moistened pores

The moistened pores i.e., the pores in which pore diffusion takes place consist of open pores reduced by the water filled pores. Hence,

$$\Psi_{diff} = b \cdot (\Psi_{op} - \Psi_w) \quad (37)$$

The fraction of the moistened pores is, therefore, a function of the water content (u).

Between water content zero (dry material) and the free saturation (u_{fs}), the parameter b can take values between 0 and 1. For free water saturation b becomes 1. If the free saturation water content (u_{fs}) is equal to the maximum water content, which applies in the case of open-porous materials such as mineral wool, no air remains in the pores of the material. Consequently, the fraction of moistened pores $\Psi_{op} - \Psi_w$ and thus Ψ_{diff} is zero: no pore diffusion takes place.

The fraction b has to be determined by iterative curve-fitting using e.g., the Nelder–Mead algorithm [38]. For each data set of thermal conductivity as a function of temperature and moisture content (u) the corresponding b value has to be determined.

For the predictions of b as a function of water content (u) the following empirical correlation developed by Krischer [36] is suggested in the VDI Heat Atlas ([41], chapter Mg 11):

$$b = 1 - \left(1 - \frac{u}{u_{fs}}\right)^9 \quad (38)$$

Only a small database is available to prove this correlation (i.e., in [36]). As b, the fraction of moistened pores, in Eq. (38) only depends on the free saturation water content, only one curve is shown in a diagram of b vs. the normalized water content (u/u_{fs}) for all materials. However, the present measurements indicate that the fraction of pores (b) in which pore diffusion takes place does not depend on the free saturation water content only. Therefore, a more complex correlation may be required.

The development of b as a function of the water content (u) is similar to the development of the water retention curve $u(\phi)$ of porous materials. Thus, already known correlations may be applied. A one-parameter approach (model II) is given with Eq. (39) from [49] while better results can be achieved using Eq. (40), suggested in [50].

$$b = \frac{u \cdot c}{u_{fs} \cdot (1 - c) + u} \tag{39}$$

$$b = \exp\left(m_1 \cdot \left(\frac{u_{fs}}{u} - 1\right)^{m_2}\right) \tag{40}$$

The comparison of the predictions of the three models and the experimental data (iteratively determined data $b(u)$ for expanded glass granules 4–8 mm and expanded clay 4–8 mm) is shown in Fig. 8. Best agreement between model prediction and experimental data is obtained using model III, Eq. (40). The temperature and water content dependency of Ψ_{diff} using Eq. (40) is illustrated in Fig. 9 for expanded glass granules 4–8 mm type II.

3.7. Temperature dependence of the closed pore fraction

Per definition, closed pores are not accessible to water. Due to the decreasing viscosity (η) and surface tension (σ) of water with increasing temperature, the fraction of not accessible pores is assumed to decrease with increasing temperature according to the following equation.

$$\Psi_{cl}(\vartheta) = \chi \cdot \Psi_{cl,ref} \cdot \frac{\eta(\vartheta)}{\eta_{ref}} \cdot \frac{\sigma(\vartheta)}{\sigma_{ref}} \tag{41}$$

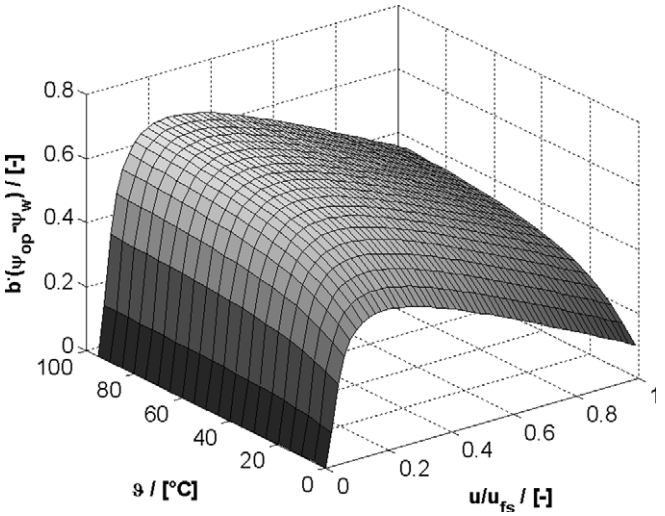

Fig. 9. Fraction of moistened pores ($b \cdot (\Psi_{op} - \Psi_w)$) as a function of temperature (ϑ) and normalised water content (u/u_{fs}).

The dynamic viscosity and the surface tension can be approximated by polynomials according to [43]:

$$\eta(T) = a_0 + a_1 \cdot T + a_2 \cdot T^2 + a_3 \cdot T^3 + a_4 \cdot T^4 \tag{42}$$

with

$$a_0 = +0.465625$$
$$a_1 = -0.00538585$$
$$a_2 = +2.34689 \cdot 10^{-5}$$
$$a_3 = -4.55704 \cdot 10^{-8}$$
$$a_4 = +3.32314 \cdot 10^{-11}$$

$$\sigma(T) = 0.09429 + 4.530 \cdot 10^{-6} \cdot T - 2.663 \cdot 10^{-7} \cdot T^2 \tag{43}$$

The temperature dependency of viscosity and surface tension are shown in Fig. 10. The temperature dependence of the fraction of open and closed pores of expanded glass granules 4–8 mm type II, calculated with Eq. (41) is additionally depicted. By setting χ in Eq. (41) equal to 0.5, good agreement between calculated and experimental results can be achieved.

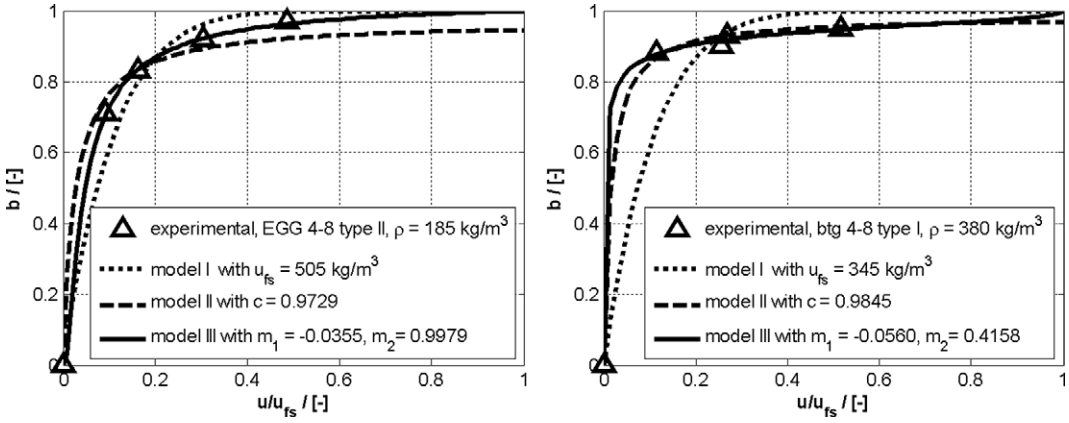

Fig. 8. Comparison of model predictions and agreement with experimental results for the fraction of moistened pores (b) for expanded glass granules 4–8 mm type II (EGG: left) and expanded clay 4–8 mm type I (EC: right).

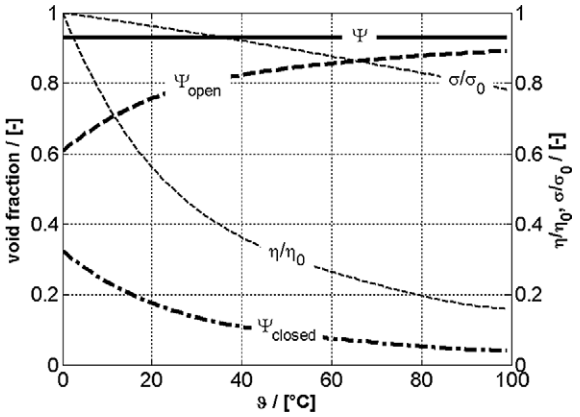

Fig. 10. Fraction of open pores (Ψ_{open}) and closed and thus for water inaccessible pores (Ψ_{closed}) as a function of temperature (ϑ), temperature dependency of dynamic viscosity (η) and surface tension (σ) of water.

3.8. Measurements and model validation

The effective thermal conductivities of 11 different bulk insulation materials (see Section 2) have been measured in a temperature range between 20 °C and 80 °C for water contents between 0 and the free saturation water content (u_{fs}) with a guarded heating plate device according to DIN 52612 [51] or ASTM C 177 [52], respectively. Two identical specimens are required for each measurement with the heating plate device, which has a measurement area of $A = 500\ \text{mm} \times 500\ \text{mm}$ with a 200 mm guard ring. The height of the specimens is 70 mm for most insulation materials. However, a specimen height of 100 mm has been chosen for insulation materials with coarse grains such as foam glass gravel in order to reduce the influence of the walls. Every specimen is measured in an oven-dry condition and at least at three different moisture contents. In order to guarantee mass conservation, the specimens are packed in stainless steel boxes. The loss of mass due to diffusion through the seam of the box has been determined for each measurement by weighing the specimens before and after the measurement. During all measurements, the maximum amount was below 5%, in average the difference was below 1%. The measured results are reproducible even though it is difficult to prepare the specimens with identical degree of compaction and water content.

The measurements of the thermal conductivity of the dry specimens have been conducted with a temperature difference of 10 K according to the standard. In order to minimize moisture transport during the measurements, a temperature difference between the heating plate and the cooling plate of approximately 5 K has been chosen. Nevertheless, there is some moisture transport during the measurement, which the described method does not account for. However, by means of simulation of coupled heat and moisture transfer, it can be demonstrated that the influence may be neglected.

With the commercial tool WUFi, which is based on the work of Künzel [49] simulations have been conducted. As boundary conditions measured temperatures of the heating plate and the cooling plate of a typical measurement have been used (see Fig. 11). For the simulation of the moisture transfer, a water vapour diffusion resistance factor of $\mu = 3$ has been assumed. Capillary or liquid water transport has not been considered. Furthermore, the thermal conductivity of $\lambda = 0.08\ \text{W/(m K)}$ has been increased linearly with increasing moisture content to $\lambda = 1.0\ \text{W/(m K)}$ at saturation water content of $u = 500\ \text{kg/m}^3$. Temperature-dependent modelling is not implemented.

Significant changes of the water content cannot be observed. Only at the edges, 1 cm from the hot and cold plate, respectively, the water content varies significantly. After about 20–24 h, when steady state is assumed, the measurement for the target temperature is accomplished. The heating and the cooling plate are heated to reach the next target temperature. As the cooling plate is heated faster than the heating plate, the direction of the moisture transport turns and thus, the distribution of the moisture

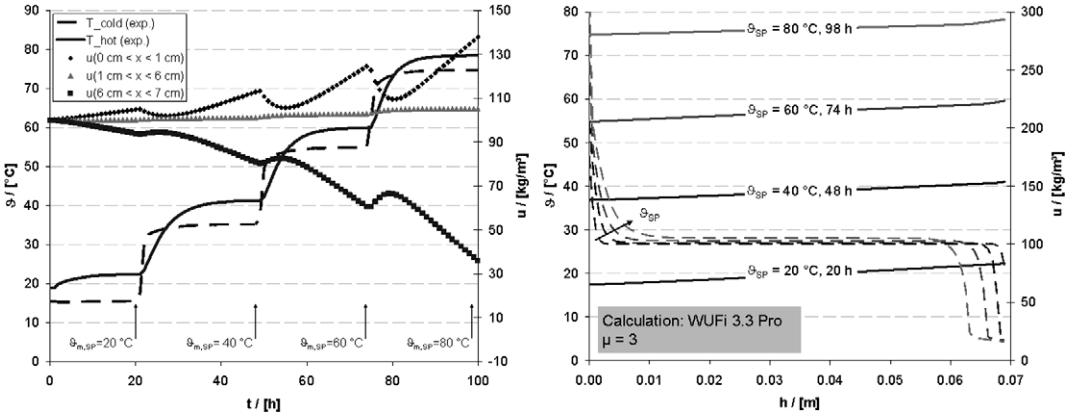

Fig. 11. Left hand side: history plot of a typical measurement of the thermal conductivity for a moist specimen ($u = 100\ \text{kg/m}^3$) with target temperatures at 20 °C, 40 °C, 60 °C and 80 °C. Measured hot plate and cold plate temperature T_{hot} (exp.), T_{cold} (exp.) and simulated moisture content u in a 1 cm layer next to the hot plate, in a 5 cm layer in the middle of the specimen and in a 1 cm layer next to the cold plate; right hand side profile plot of the temperature and the moisture content at selected times.

content equalizes before the heating plate reaches target temperature. Consequently, assuming initial moisture content for all target temperatures will not lead to major errors.

The implicitly determined coefficients m_1 and m_2 are summarised in Table 7. In Fig. 12, model predictions are compared with measured results for expanded glass granules 4–8 mm type II and expanded clay 4–8 mm type I.

Table 7
Free saturation water content (u_{fs}) and coefficients m_1 and m_2 according to Eq. (40)

Material	Grain size d (mm)	Density ρ (kg/m^3)	Free saturation u_{fs} (kg/m^3)	Eq. (40)		Eq. (39)
				m_1 (–)	m_2 (–)	c (–)
Expanded glass						
EGG type I	2–4	200	550	−0.0445	1.0334	0.9564
EGG type II	2–4	190	515	−0.0142	1.1460	0.9842
EGG type II	4–8	185	500	−0.0355	0.9979	0.9729
EGG type II	8–16	150	400	−0.1314	0.6659	0.9473
Expanded clay						
EC type I	4–8	270	300	−0.0033	2.9097	0.9662
EC type I	4–8	380	345	−0.0560	0.4158	0.9845
EC type I	1–4	340	360	−0.0431	0.7240	0.9803
EC type II	0–1	300	360	−0.0114	1.4563	0.9763
Expanded perlite						
EP type I	0–1	100	370	−0.0248	1.5487	0.9649
Foam glass						
FGG type I	10–20	155	460	−0.0145	1.6873	0.9520
GFG type II	10–50	195	150	−0.01961	2.3423	0.9292

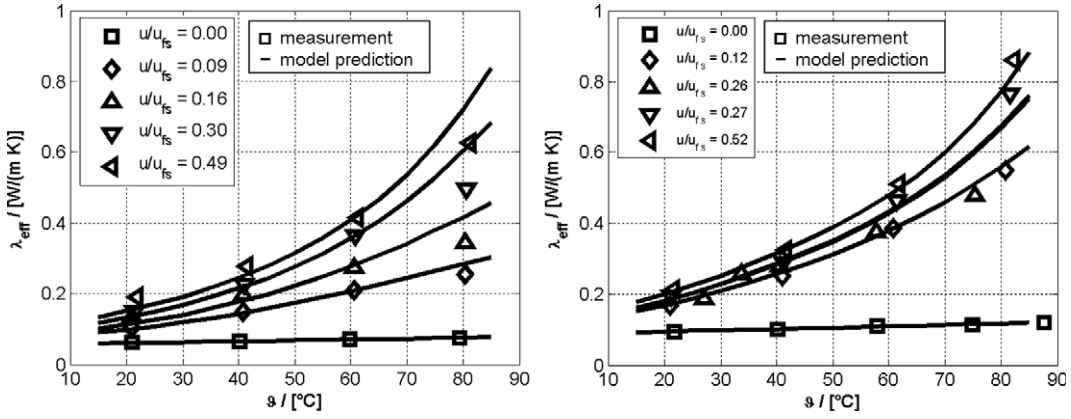

Fig. 12. Model predictions and measured data for the thermal conductivity (λ_{eff}) of expanded glass granules 4–8 mm type II (EGG: left) and expanded clay 4–8 type I (EC: right) as a function of the temperature (ϑ) with normalised water content (u/u_{fs}) as parameter.

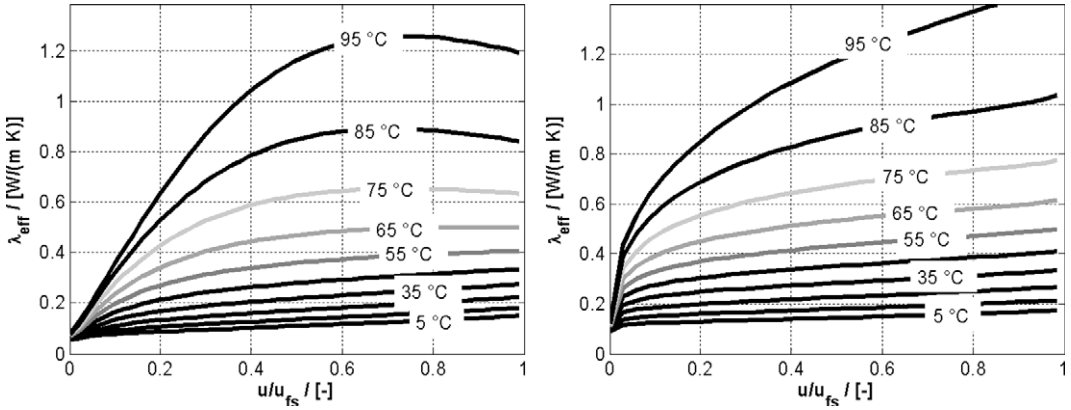

Fig. 13. Model predictions for the effective thermal conductivity of expanded glass granules 4–8 mm type II (left) and expanded clay 4–8 type I (right) as a function of the normalised water content (u/u_{fs}) with temperature (ϑ) as parameter.

Good agreement is obtained in the relevant temperature range. Nevertheless, there are deviations at 80 °C. At higher temperatures heat losses from the guarded heating plate device to the ambient result in a measured value of the thermal conductivity that is too low.

Above moisture contents of about 50 kg/m^3 (corresponding to $u/u_{fs} = 0.1$ or about 5 vol.%), an exponential increase of the thermal conductivity with increasing temperature can be recognised. Fig. 13 shows model predictions of the effective thermal conductivity of both materials as a function of the normalised water content (u/u_{fs}). For expanded glass granules, the effective thermal conductivity exceeds the value of 0.08 W/(m K) according to DIN 4108 (dry, 10 °C) by a factor of five at a temperature of 60 °C and a moisture content of about 200 kg/m^3 (20 vol.%) and at 80 °C even by a factor of 10. A similar behaviour can be recognised in the case of expanded clay.

4. Conclusions

Published information about the thermal conductivity of moistened insulation materials is sparse. Especially porous bulk insulation with partially closed pores has not been considered in previous research activities although it is increasingly applied for heat storage applications and in the building sector. Almost no measured data of the thermal conductivity of insulation materials can be found for higher temperatures. Therefore, measurement results and modelling approaches of the effective thermal conductivity of different porous bulk materials suitable for insulation have been presented in this work. Using the models for the thermal conductivity, suggested in the VDI Heat Atlas [30,41] agreement of measured and predicted thermal conductivity as a function of temperature and moisture content is insufficient. Hence, modifications to the model developed by Krischer and Kast [36] have been necessary. The model suggested in this work represents an improvement with respect to the consideration of closed pores $\Psi_{cl} = f(\vartheta)$ and the enhanced consideration of the fraction of moistened pores $b = f(u_{fs})$.

Material properties such as the free water saturation content and the fraction of open and closed pores, which represent important input parameters for the modified model, have been determined for different bulk insulation materials. By using simplified methods with reasonable effort, good results could be obtained. With the modified model for the thermal conductivity, good agreement between calculated and measured values can be obtained in the temperature range from 20 °C to 80 °C.

The introduction of a material-specific relation between the fraction of moistened pores and the water content may replace the correlation suggested in the VDI Heat Atlas [30,41] which is using the free saturation content only. A strong increase of the effective thermal conductivity at higher temperatures (>60 °C) at already small water contents (<5%) could be detected. It is obvious that the prediction of thermal losses (and thus, the sizing of the insulation thickness) using the values recommended in DIN 4108 [12] will result in significant errors. In comparison to manufacturer or DIN specifications, which are given for 10 °C, in real operation the effective thermal conductivity and thus, the thermal losses can be higher by a factor of 4–10.

Measured thermal losses of buried heat stores with operating temperatures up to 100 °C may be explained by increased values of the effective thermal conductivity due to moistened insulation.

The transient simulation of the coupled heat and moisture transfer becomes increasingly important. The majority of related publications have their origin in the building sector (i.e., determination of hygric and thermal performance of building structure or risk of mould growth). In all published papers (i.e., [42,43,49,53–55]) the temperature influence of the thermal conductivity has not been considered. In some simulation programmes, the thermal conductivity is considered to be constant. However, the experimental and modelling results presented in this paper demonstrate that the influence of elevated temperatures and moisture should be considered when conducting heat and moisture transfer simulations for these conditions.

Acknowledgements

The results presented in this paper have been obtained in the framework of the project "Further Development of the Pit Heat Storage Technology". The project is supported by the German Federal Ministry for the Environment, Nature Conservation and Nuclear Safety (Bundesministerium für Umwelt, Naturschutz und Reaktorsicherheit), FKZ 0329607E.

References

[1] E. Hahne, M. Benner, D. Mangold, T. Schmidt, M.E. Schulz, Solare Nahwärme - Ein Leitfaden für die Praxis, Fachinformationszentrum Karlsruhe (BINE), TÜV-Verlag, Köln, 1998.
[2] M. Benner, B. Mahler, D. Mangold, T. Schmidt, M. Schulz, H. Seiwald, Solar unterstützte Nahwärmeversorgung mit und ohne Langzeit-Wärmespeicher, Forschungsbericht zum BMBF-Vorhaben (September 1994 bis Oktober 1998), ISBN-Nr. 3-9805274, 1999.
[3] M. Benner, M. Bodmann, D. Mangold, J. Nußbicker, S. Raab, T. Schmidt, H. Seiwald, Solar unterstützte Nahwärmeversorgung mit und ohne Langzeit-Wärmespeicher, Forschungsbericht zum BMBF-Vorhaben (November 1998 bis Januar 2003), ISBN-Nr. 3-9805274-2-5, 2004.
[4] M. Bodmann, D. Mangold, J. Nußbicker, S. Raab, A. Schenke, T. Schmidt, Solar unterstützte Nahwärme und Langzeit-Wärmespeicher, Forschungsbericht zum BMWA / BMU-Vorhaben (Februar 2003 bis Mai 2005), Stuttgart, 2006.
[5] IEA Task VII, Central Solar Heating Plant with Seasonal Storage, Status Report, Stockholm, ISBN 91-540-5201-7, 1990.
[6] IEA Task XIV, Advanced Active Solar Systems, Working Group "Large Solar Energy Systems", Final IEA Report, No. T.14.LS.1, Delft, 1996.
[7] J.-C. Hadorn, Guide to seasonal heat storage, SIA Documentation D 028 in the series Planning Energy and Buildings, 1988.
[8] A. Heller, Development of seasonal storage, in: Denmark: Status of storage programme 1997–2000, Terrastock 2000, Stuttgart, 2000, Proceedings, S. 47–52.

[9] P.A. Sørensen, Final Technical Report, Solar thermal and long term heat storage for district heating systems, Sunstore 2, Marstal, 2005.
[10] J.O. Dalenbäck, Solar Heating with seasonal storage – some aspects of the design and evaluation of systems with water storage, Ph.D Thesis, Chalmers University of Technology, Göteborg, 1993.
[11] T. Schmidt, D. Mangold, New steps in seasonal thermal storage in germany, ecostock 2006, Richard Stockton College of New Jersey, 2006.
[12] DIN V 4108-4, Thermal insulation and energy economy in buildings, hygrothermal design values, 2004.
[13] A. Heller, Floating lid constructions for large pit water heat storage, Megastock 1 (1997) 503–508.
[14] S. Raab, D. Mangold, W. Heidemann, H. Müller-Steinhagen, Solar assisted district heating system with seasonal hot water heat store in Friedrichshafen (Germany), in: Proceedings of EuroSun 2004 – The Fifth ISES Europe Solar Conference, 20–23 June 2004, Freiburg, Germany, 2004.
[15] J. Bühl, Langzeitwärmespeicherung mit einem neuartigen Speicherkonzept, FVS Workshopband, Köln, 2001.
[16] M. Schlosser, Solar unterstützte Nahwärmeversorgung Hannover Kronsberg, OTTI, 16. Symposium Thermische Solarenergie, Kloster Banz, Bad Staffelstein, 2006.
[17] S. Raab, D. Mangold, W. Heidemann, H. Müller-Steinhagen, Solar assisted district heating system, in: Crailsheim (Germany), Proceedings of Solar World Congress, Orlando (USA), 06.-12.08.2005, Orlando, 2005.
[18] D. Mangold, Die neuen Pilotprojekte mit Langzeit-Wärmespeicher, OTTI, 16. Symposium Thermische Solarenergie, Kloster Banz, Bad Staffelstein, 2006.
[19] R. Giebe, Ein Kies/Wasser-Wärmespeicher, in: Praxis und Theorie, Dissertation, Universität Stuttgart, 1989.
[20] T. Urbaneck, Berechnung des thermischen Verhaltens von Kies-Wasser-Speichern, Dissertation, TU Chemnitz, 2003.
[21] M. Pfeil, H. Koch, Saisonaler Kies/Wasser-Wärmespeicher der 3. Generation für die Solarsiedlung Steinfurt Borghorst, OTTI, 10. Symposium Thermische Solarenergie, Kloster Banz, Bad Staffelstein,1999, Tagungsband, S. 59–63, 1999.
[22] M. Bodmann, M.N. Fisch, Betriebserfahrungen der solar unterstützten Nahwärmeversorgung in Hannover, Steinfurt und Hamburg, OTTI, 13. Symposium Thermische Solarenergie, Kloster Banz, Bad Staffelstein, 2003.
[23] P.A. Sørensen, SUNSTORE 2, Monitoring results from the project and construction of 10000 m^3 pit heat storage, Sunstore 2 Workshop, September 2004, Marstal, Aero, 2004.
[24] F. Ochs, W. Heidemann, H. Müller-Steinhagen, H. Koch, Effective thermal conductivity of the insulation of high temperature underground thermal stores during operation, ecostock 2006, Richard Stockton College of New Jersey, 2006.
[25] J. Hurley, A UK market survey for foam glass, research and development final report, GLA 0015, The Waste and Resources Action Programme, 2003.
[26] T. Faust, M. Beck, Pore structure of different LWAs, Summary 1999, Universität Leipzig, 1999.
[27] A. Bouguerra, J.P. Laurent, M.S. Goual, M. Queneudec, The measurement of the thermal conductivity of solid aggregates using the transient plane source technique, J. Phys. D. Appl. Phys. 30 (1997) 2900–2904.
[28] DIN 66133, Determination of the pore volume distribution and the specific surface area of solids by mercury intrusion, 1993.
[29] DIN 66135, Micropore analysis by gas adsorption, Part 4. determination of pore size distribution according to the Horvath–Kawazoe and Saito–Foley method, 2001.
[30] E. Tsotsas, VDI- Wärmeatlas, Kapitel Dee, 9. Auflage, Springer Verlag, 2002.
[31] H. Saechtling, K. Oberbach, Kunststofftaschenbuch, 28. Auflage, Hanser Verlag, 2001, ISBN 3-446-21605-7.
[32] H.D. Baehr, K. Stephan, Wärme- und Stoffübertragung, 2. Auflage, Springer Verlag, Berlin, 1996.
[33] K. Walz, (Schriftleitung), Merkblatt I für Leichtbeton und Stahlbeton, Betontechnische Berichte des Forschungsinstituts der Zementindustrie.
[34] DIN EN 13755, Determination of water absorption and saturation coefficient, 2002.
[35] P. Zehner, Experimentelle und theoretische Bestimmung der effektiven Wärmeleitfähigkeit durchströmter Kugelschüttungen bei mäßigen und hohen Temperaturen, Diss., Uni Karlsruhe, Fakultät für Chemieingenieurwesen 1972.
[36] O. Krischer, W. Kast, Die wissenschaftlichen Grundlagen der Trocknungstechnik, 3. Auflage, Springer-Verlag, Heidelberg, 1992.
[37] M.G. Zeitler, Allgemeingültiges Modell zur Berechnung der Wärmeleitfähigkeit poröser Stoffe und Stoffschichten, Diss., Uni Essen, 2000.
[38] J.A. Nelder, R. Mead, A Simplex method for function minimization, Comput. J. 7 (1965) 308–313.
[39] U. Quast, Wärme- und Stoffübertragung in Gegenstrom-Kühltürmen unter Berücksichtigung von Nebel- und Sprühtropfenbildung, TH Darmstadt, Dissertation, 1977.
[40] D. Ackermann, Wärme- und Stoffübertragung bei der Kondensation eines turbulent strömenden Dampfes in Anwesenheit von Inertgas, Dissertation, Universität Stuttgart, Stuttgart, 1972.
[41] E. Tsotsas, VDI-Wärmeatlas, Kapitel Mg 11, 9. Auflage, Springer-Verlag, 2002.
[42] D.A. De Vries, Heat transfer in soils, in: W.R. Van Wijk (Ed.), Phys. Plant Environ., North Holand Publishing, Amsterdam, 1966.
[43] T. Bednar, Beurteilung des feuchte- und wärmetechnischen Verhaltens von Bauteilen und Gebäuden, Weiterentwicklung der Meß- und Rechenverfahren, Dissertation, TU Wien, Wien, 2000.
[44] R. Schirmer, Die Diffusionswiderstandszahl von Wasserdampf-Luftgemischen und die Verdampfungsgeschwindigkeit, VDI Beiheft Verfahrenstechnik 6 (1938) 170.
[45] M. Krus, Feuchtetransport und Speicherkoeffizienten poröser mineralischer Baustoffe. Theoretische Grundlagen und neue Messtechniken, Dissertation, Lehrstuhl Konstruktive Bauphysik, Uni Stuttgart, Stuttgart, 1995.
[46] A.-C. Andersson, Verification of calculation methods for moisture transport in porous building materials, Swedish Council for Building Research, D6: 1985, Stockholm, 1985.
[47] D. Sonntag, D. Heinze, Sättigungsdampfdruck- und Sättigungsdampfdichtetafeln für Wasser und Eis. (1. Aufl.), VEB Deutscher Verlag für Grundstoffindustrie, 1982.
[48] R.C. Reid, J.M. Prausnitz, B.E. Poling, The Properties of Gases and Liquids, Third ed., McGraw-Hill Book Company Inc., New York, 1977.
[49] H.M. Künzel, Verfahren zur ein- und zweidimensionalen Berechnung des gekoppelten Wärme- und Feuchtetransports in: Bauteilen mit einfachen Kennwerten, Lehrstuhl Konstruktive Bauphysik, Uni Stuttgart, Stuttgart, 1994.
[50] A. Holm, M. Krus, H.M. Künzel, Approximation der Feuchtespeicherfunktion aus einfach bestimmbaren Kennwerten, IBP-Mitteilungen 406, 29 (2002), Fraunhofer Institut für Bauphysik (IBP), Stuttgart, 2002.
[51] DIN 52612, Bestimmung der Wärmeleitfähigkeit mit dem Plattengerät, in German, 1979.
[52] ASTM C 177, Guarded Hot Plate Method, 1993.
[53] P.C. Rode, Combined heat and moisture transfer in building constructions, Dissertation, DTU, Denmark, 1990.
[54] J. Grunewald, Diffusiver und konvektiver Stoff- und Energietransport in kapillarporösen Baustoffen, Dissertation, Technische Universität Dresden, Dresden, 1997.
[55] M. Deru, A model for ground coupled heat and moisture transfer from buildings, NREL/TP-550-33954, 2003.